Contents lists available at ScienceDirect

Materials and Design

journal homepage: www.elsevier.com

Design of multilayer Cr-CrN thin coatings with tailored residual stress profiles

Marco Renzelli, Muhammad Zeeshan Mughal, Marco Sebastiani *, Edoardo Bemporad

"Roma Tre" University, Engineering Department, Via della Vasca Navale, 79, 00146 Rome, Italy

ARTICLE INFO

Article history:
Received 8 July 2016
Received in revised form 25 August 2016
Accepted 15 September 2016
Available online xxx

Keywords:
Multilayer
Coating
Residual stress
Scratch
Focused ion beam

ABSTRACT

Compressive residual stress in hard coatings can improve adhesion and in-service toughness, since they can inhibit crack nucleation and propagation. However, the role of through thickness residual stress profile is not fully understood. This is because of (a) lack of knowledge of stress evolution mechanisms and (b) limitations of experimental techniques used for stress profiling.

The present work deals with design, deposition and characterization of Cr-CrN multilayer coatings, produced by Magnetron Sputtering Physical Vapour Deposition (MS-PVD).

Analytical modelling was used to determine the optimal residual stress distribution for a range of contact loading situations. On the basis of modelling activities, three different Cr-CrN multilayers were produced, with the aim of obtaining different stress gradients, as measured by incremental micro-scale focused ion beam (FIB) ring-core method, while keeping the same average stress value and same average hardness in the film.

Results show a significant correlation between the observed residual stress profiles and scratch adhesion, where different optimal stress profiles are identified for different loading conditions. In particular, we show that a lower interfacial compressive stress and a reduced through thickness stress gradient gives improved scratch adhesion, when using 10 μm and 200 μm sphero-conical indenters.

1. Introduction

Compressive stresses in hard coatings [1] can inhibit crack propagation, enhancing the apparent toughness [2,3]; however high stresses near the coating/substrate interface can induce buckling and delamination of the film [4]. Both analytical and numerical models indicates the possibility to increase the coating performance by "tuning" the compressive stress profile inside the film, both in terms of average magnitude and gradient through the thickness, with respect to a specific tribological or loading situation [2,4–7].

The recent development of residual stress profiling procedures [8] allow researchers to verify the actual variation of the residual stress through the film thickness, in order to look for correlations between the stress variation and the mechanical behaviour. In particular, residual stress assessment at the micrometer scale using focused Ion beam (FIB) milling [9–11] has evolved into a promising technique to evaluate incremental stress relaxation, thus enabling to study stress gradients along the coating thickness [10]. The ability of measuring the residual stress profiles in thin films can open the way to the actual design (or fine tuning) of residual stress profiles to increase the adhesion and wear resistance.

Until now, it is not known how to increase the coating performance through modelling and controlling the through thickness stress profiles. There is no specific literature available, which present a careful design of stress profiles to obtain maximum performance in a given contact condition, without changing hardness and/or stiffness of the film. A possible approach to control and optimise residual stress in hard coatings is to design a multilayer structure made of alternating metal/ceramic layers. In a previous paper [12], the authors have demonstrated that optimal positions and thickness metal/ceramic layers can be carefully designed in Ti-TiN multilayer systems, to improve adhesion without affecting the hardness of the coating. An example of the optimal multi-layer system is reported in Fig. 1.

However, the effects of stress profiles in the different TiN layers on adhesion was not taken into account, even though it was clear that changes in the mechanical behaviour of the films were clearly related to changes of the residual stress distributions.

On this basis, the main objective of the present work is to assess the effects of a residual stress profile on scratch adhesion of a given multi-layer coating. Basing on analytical optimisation algorithm of the elastic contact stress fields [13], we have designed the optimal desirable residual stress profile in the film under different loading conditions. A number of Cr-CrN coatings were then designed, produced and subsequently fully characterised.

Results showed that (1) different optimal stress profiles should be sought for different tribological situations and (2) residual stress profiles can affect dramatically the scratch adhesion of a ceramic coating, while all other parameters (thickness, microstructure, texture, hardness) are kept constant.

2. Analytical modelling and coating design

The main objective of the analytical modelling was to assess the effect of a residual stress profile on the mechanical behaviour of a coated system under contact with a spherical indenter and different applied loads. Additionally, an optimisation algorithm is exploited, in order to find the optimal residual stress profile (i.e. the one giving

* Corresponding author.
Email address: marco.sebastiani@uniroma3.it (M. Sebastiani)

http://dx.doi.org/10.1016/j.matdes.2016.09.058
0264-1275/

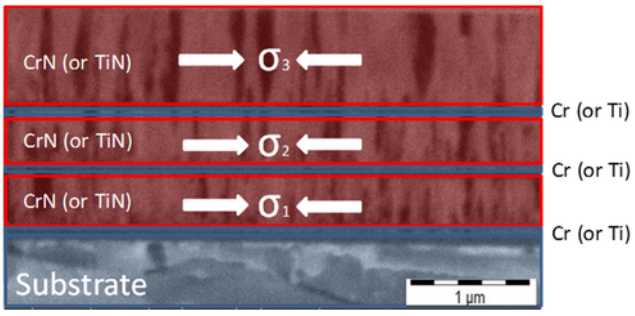

Fig. 1. Multilayer architecture proposed in a previous paper [12]. Design of stress profile in the three layers is proposed in this work.

minimum interfacial contact stress peak) for a range of indenter radii and applied loads.

Analytical calculations were performed using a purposely developed intrinsic stress optimization module within the analytical modelling software package (FilmDoctor®) [14]. The software allows for the analytical calculation of the elastic contact stress distribution in coatings, by using an extended Hertzian theory that was presented in previous paper [13]. The optimization algorithm presented here, works in a way of reducing a given stress component (or even the von Mises equivalent stress), while optimally distributing, by iterations, the intrinsic stress profiles within the coating thickness.

In order to investigate a wide range of loading conditions, a number of simulations were performed by varying the indenter radius as well as the applied load/force. Fig. 2 highlights one example of those simulations, showing a 3 µm CrN coating on a steel substrate under a 200 µm radius diamond indenter with the application of 500 mN force. After the optimization, the same coating was divided into 5 equal parts (highlighted by the white dashed lines), to which the optimal residual stress distribution is obtained after iteration. In this way, the resulting von Mises stress (indicated by the arrow) was significantly reduced for this particular load scenario.

The same optimisation was repeated for a wide range of indenter radii and applied loads: Fig. 3 highlights the optimal distribution of intrinsic stresses for different tip radii (10 µm to 300 µm) with loads ranging from 50 to 500 mN.

In more detail, the following observations can be drawn from Fig. 3:

- It is evident from Fig. 3, that changing load condition from 50 mN to 500 mN, completely changes the desired optimal stress profile.
- Point loading situations, obtained by small indenter radii and lower applied loads, would require higher surface residual stresses and lower interfacial residual stresses;
- Situations where contact area is large, obtained by large indenter radius and high applied loads, would require higher interfacial stress;
- Smaller indenter radius requires both high average as well as high gradient of stress in the coating regardless of the load.
- Combination of smaller indenter radius and high load requires high value of average stresses throughout the thickness of the coating, while smaller radius and low load requires high gradient of stresses in the coating.

Please note that the above conclusions are obtained by only seeking for minimisation of the von Mises elastic stress in the film under different contact situations; neither assumptions on possible buckling of the film because of compressive stress, nor plasticity in the substrate are taken into account by the software.

A good way to validate the performance of optimization algorithm, is the production and characterization of demonstrators with completely different stress profiles while keeping the same thickness and/or microstructure. The main idea was to have two coatings with completely opposite stress profile, i.e. one with the high surface/low

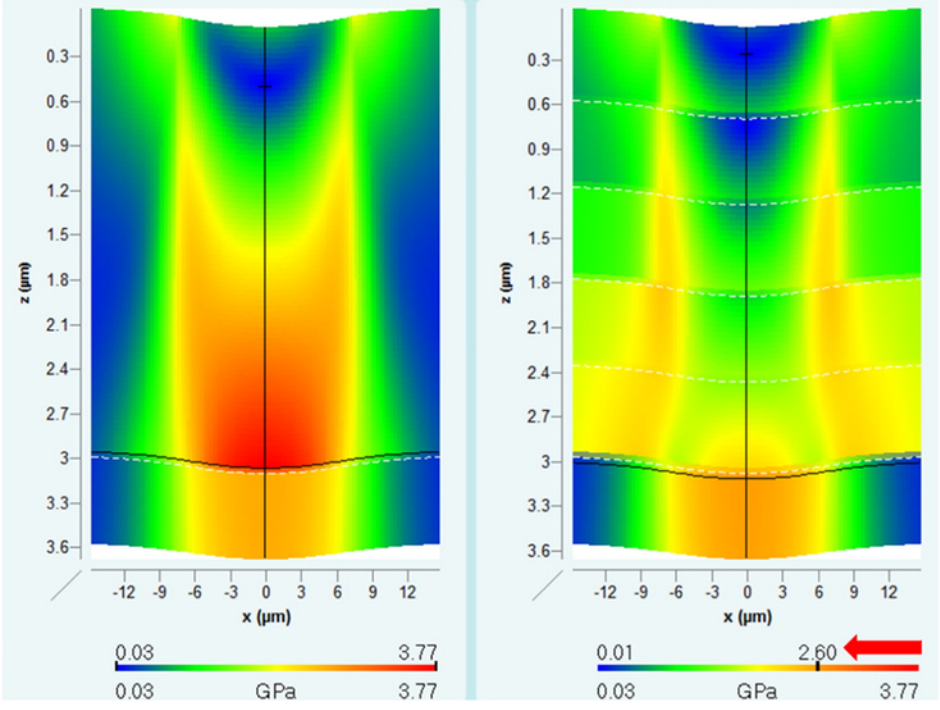

Fig. 2. CrN coating on steel substrate under a diamond indenter, before optimization (left) and after optimization of the residual stress profile (right). The arrow indicates the reduction in von Mises stresses after optimization.

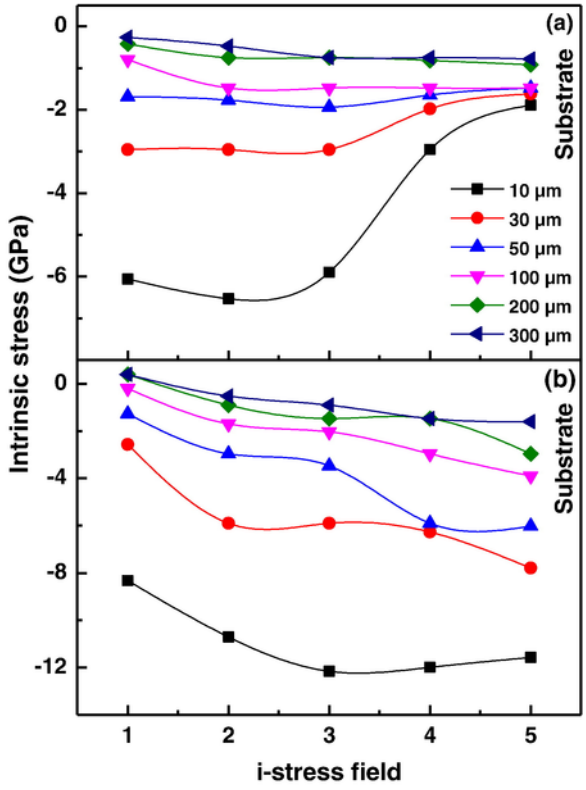

Fig. 3. A 3 μm CrN coating under different indenter radii and load: (a) 50 mN and (b) 500 mN. The intrinsic stress (i-stress) field represents the distinctive positions within the optimized coating thickness.

interface stress and one with low surface/high interface stress. Since the production of coatings with similar microstructure but different stress profiles is not an easy task, the activity was planned to first study the structure-stress relationship on a given coating system (namely, CrN). From the results of the stress assessment and microstructural analysis of the single-layers, it was possible to make a correlation between process parameters and resulting stress profiles, hence achieving coatings with known stress profile.

3. Experimental details

3.1. Single-layer coating deposition

All CrN coatings used in this study were deposited on AISI 304 steel substrates, which were mirror polished and cleaned in two subsequent ultrasonic baths of acetone and ethanol. Deposition was performed by a standard DC magnetron sputtering plant using a RF induced bias. Both the samples and the cathode were sputtered cleaned for 15 min, while maintaining a base pressure of $< 6 \times 10^{-6}$ mbar. All the depositions were voltage driven to control ions energy, and thus induced stresses. To control the possible change of the current (with fixed voltage) due to target erosion, the product of deposition time and current was kept constant instead of the deposition time. Due to the high interplay of process parameters in the deposition physics, it is usually difficult to control only one property (stress) while varying only one parameter (bias). To achieve this result, the gas mix parameters with a high reactive gas content were chosen to poison the target ensuring similar coating composition from one deposition to another. For all cases reported here, reactive gas mix and cathode voltage were the same (Table 1), while the bias voltage on the sample was varied to change the average stress inside the coating. All coatings were deposited on a chromium bond-layer with a thickness of 0.1 μm, which is known to increase the adhesion of the coating to the substrate [15].

Table 1
Gas flow and cathode voltage used for all depositions.

Parameter	Quantity
Ar flow (sccm)	*40*
N_2 flow (sccm)	*100*
Cathode DC bias (− V) Cr Layer	*345*
Cathode RF bias (− V) CrN Layer	*80*
Cathode DC bias (− V) CrN Layer	*435*
Variable parameter: substrate bias (− V)	60–210

3.2. Multi-layer coating deposition

Three multilayer coatings were produced using the combination of bias voltage − 120, − 150 and − 180 V. The coatings are made of three CrN layers and two Cr interlayers; a Cr bond layer is between the first CrN layer and the steel substrate. It is worth noting that the deposition is not stopped on changing the bias and/or the material. Any bias and/or working gas changes are made without breaking the vacuum. The first sample was a tri-layer system with all CrN layers deposited at a bias of − 120 V which was used as a benchmark (***120_120_120***). The purpose of this coating is to see how the multilayer structure differed from the conventional monolayer grown at -120 V bias. This is followed by two different multilayer samples, one with high bias (− 180 V) in the top-layer and low bias (− 120 V) in the base layer (***180_150_120***), the other with low bias (− 120 V) in the top-layer and high bias (− 180 V) in the base layer (***120_150_180***). In both of these samples, the middle layer was produced using an intermediate bias of -150 V.

3.3. Coating characterization

3.3.1. X-ray diffraction for phase ID, stress and texture measurements

XRD measurements were made by a Bruker D8 Discover with a LinxEye XE detector and a copper anode twist-tube was used for XRD measurements, in grazing incidence ($\alpha = 3°$) line focus configuration with a Göbel mirror for phase identification and in point focus configuration with a 0.5 mm snout for texture measurements and stress assessment according to $\sin^2\psi$ technique, side inclination [16]. Orientation Distribution Function (ODF) was obtained from the pole figures of three different lattice reflections ((111), (200) and (320)) using the MatLab package MTEX [17,18].

3.3.2. Nanomechanical characterization (E, H, Kc)

Mechanical characterization (E, H) was done using instrumented nano-indentation testing, using a Nanomechanics iNANO nano-indenter fitted with Berkovich diamond indenter and operated in continuous stiffness measurement (CSM) testing, hence allowing obtaining both hardness (H) and modulus (E) as continuous function of depth from a single indentation experiment. A fused silica sample was tested before and after a batch measurement to ensure the reliability of the results. For all cases reported here, a minimum of 25 indentation were performed and the calculations were made by the Oliver and Pharr method from the load-displacement curve using 10% of the film thickness as the maximum indentation depth [19].

Fracture toughness of the coating was evaluated using the recently developed pillar splitting technique [20,21]. The method relies on

sharp indentation testing on FIB milled micro pillars which were milled to an aspect ratio of (h/d) of > 1.2, where h is the pillar height and d is the top diameter. It has been shown previously [20,21] that this geometrical design provides complete residual stress relaxation in the upper part of the pillar. The method does not require measurement of crack length and fracture toughness can be computed by only measuring the splitting load, pillar radius and hardness/modulus ratio of the coating. Eq. (1) shows the relationship used for calculating the fracture toughness values.

$$K_c = \gamma \frac{P_c}{R^{3/2}} \tag{1}$$

where K_c is the fracture toughness (MPa.m$^{1/2}$), P_c is the critical splitting load (mN) and R is the pillar radius (μm). The coefficient γ is the material specific constant and has computed for wide range of materials using the cohesive zone finite element modelling (CZ-FEM) [21]. More recent applications of the technique can be found in the following references [21–23].

The pillars were FIB milled in a single outer to inner pass at a current of 0.92 nA. The pillar indentation tests were performed on a Keysight G200 nanoindenter, using a XP indentation head at a constant strain rate of 0.05 s^{-1}. All indentation experiments were performed using a Berkovich tip with the maximum indentation depth set to 500 nm into the top surface. The instrument frame stiffness and indenter area function were calibrated before and after testing on a certified fused silica reference sample. The continuous stiffness measurement (CSM) mode was turned off during the pillar splitting experiments.

3.3.3. Focused ion beam (FIB) cross sectioning and stress profiling

Cross sectioning and ring core milling for thickness and stress measurement purposes were carried out in a FEI Helios Nanolab 600 dual beam FIB/SEM. The ring core procedure [8,10] was performed using 48pA current at 30 kV. Step by step milling was performed using an annular trench of different diameters (Fig. 4). High resolution SEM micrographs were acquired before and after every milling step using an integral of 128 images and at 50 ns dwell time while maintaining the same contrast as the reference image. Ion and electron beam drift was automatically monitored and corrected during the test. A Digital Image Correlation (DIC) [24] software was then used to obtain relaxation strain values from the micrographs. The most widely used approach for stress profiling after incremental strain measurement is the integral method, originally proposed by Schajer [25,26] for the hole drilling geometry, which assumes that the total measured relaxation strain at a certain depth ε(h) is given by the integral of the infinitesimal strain relief components due to the removal of tractions at all depths in the range 0 ≤ H ≤ h, that is:

$$\varepsilon(h) = \int_0^h A(Hh) \cdot \sigma(H) \cdot dH \tag{2}$$

Here, $\sigma(H)$ is the local stress which was present before material removal at depth H. A(H, h) is the influence function (also called Kernel function) and describes the strain caused by a unit stress at depth H within a hole of depth h. Eq. (2) holds in case of equibiaxial stress state, which is the most representative situation for the case of thin PVD coatings considered here. An effective method for solving Eq. (2) is to divide the unknown stress profile into n discrete calculation points:

$$\varepsilon_i = \sum_{j=1}^{j=i} A_{ij}\sigma_j \; 1 \le j \le i \le n \tag{3}$$

where A_{ij} is a lower triangular matrix of calibration coefficients which relates the strains relaxed at the surface when the groove has j depth increments to the principal stresses acting in the i layer and is usually obtained by finite element modelling (FEM) [8].

3.3.4. Scratch testing

The scratch tests were performed using an Anton Paar Revetest Xpress micro scratch tester, using both a 200 μm and 10 μm Rockwell diamond tips. Scratches were made using a continuously increasing load for an interval length of 10 μm. The linearly increasing load is applied from 1 to 90 N for 200 μm indenter, while 1 to 10 N load was applied in the case of 10 μm indenter. The choice of two different tip radii was made to highlight the differences between sam-

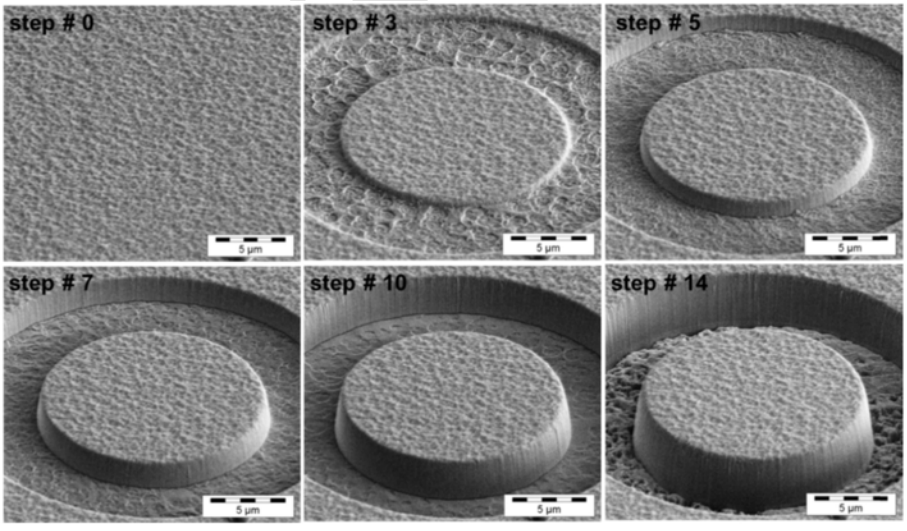

Fig. 4. Step by step FIB milling of a 15 μm pillar on a CrN coating.

ples with different residual stress profiles, since higher surface contact stresses are expected for lower indenter radii, while higher interfacial contact stresses should be obtained for a higher radius.

The critical load for first lateral chipping of the coating was determined by using the acoustic emission signal. The critical load for delamination was determined from the friction force –scratch distance plot as the point at which the first sudden change of friction coefficient is detected, and then confirmed by optical observation (according to UNI EN 1071-3 standard).

4. Results and discussion

4.1. Microstructures of the films

Fig. 5 shows the cross sectional images for − 60, − 120 and − 210 bias samples. The − 60 V bias clearly shows the presence of fine grains throughout the thickness of the coating (Zone I of the Thornton's Structure Zone Model, SZM), while − 120 V and − 210 V represents the conventional columnar, "V shape" structure for these coatings (Zone T of the SZM) [27].

Fig. 6 highlights the cross sectional images of all the multilayer coatings, showing that all the samples have the same layer structure and the grains pass through the CrN-Cr-CrN interfaces without disruption and re-nucleation.

The grain growth in all the multilayer samples can easily be characterised in Zone T [27], with "V" shape grains, smaller near the interface and bigger at surface. The typical stress evolution in these coatings class is a gradient from the interface (high stress) to the surface (low stress).

Fig. 7 reports the grazing incidents diffraction plots of all the CrN single layer coatings. Two peaks namely (111) and (200) are clearly visible, confirming the presence of face-centred cubic (fcc) structure [28–30]. Variation in the substrate bias voltage affects the crystallographic texture of CrN films. It is clear from Fig. 7 that up to a bias voltage of − 100 V, film structure exhibits mixed (111) and (200) peaks [29]. Above − 120 V bias voltage, a preferred (111) orientation is observed [29] and is consistent up to the maximum bias of − 210 V.

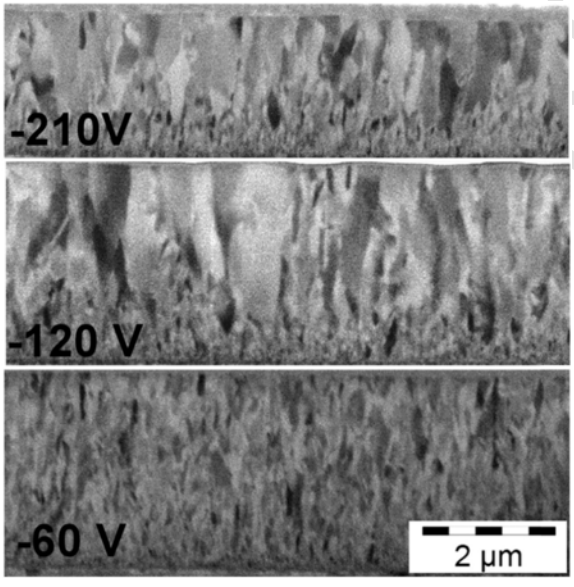

Fig. 5. FIB cross sectional images of monolayer coatings at three different biases.

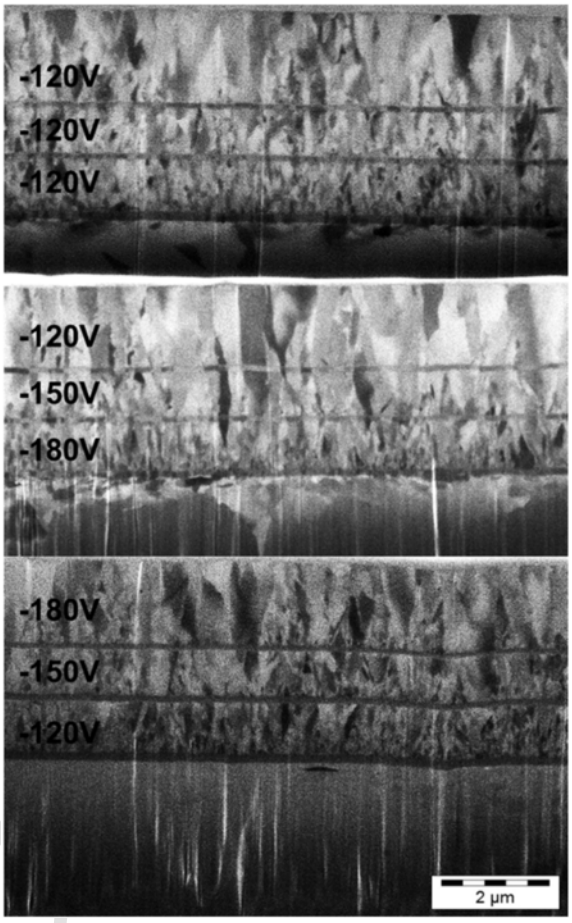

Fig. 6. FIB cross sections of the three multilayer samples, showing similar layer structure, grain size and grain growth (Zone T coatings). Thin horizontal lines represents Cr interlayers.

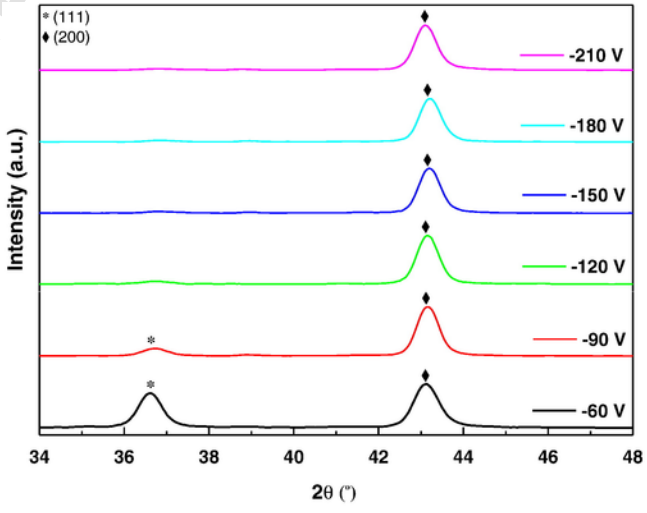

Fig. 7. X-Ray diffraction patterns of CrN coating grown at different bias voltage.

This microstructure difference was quantified making pole figures of three not parallel lattice reflection (i.e. 111, 200, and 220) and using the MatLab software MTEX to evaluate the Orientation Distribution Function (ODF). Fig. 8 shows the pole figures of low-bias and

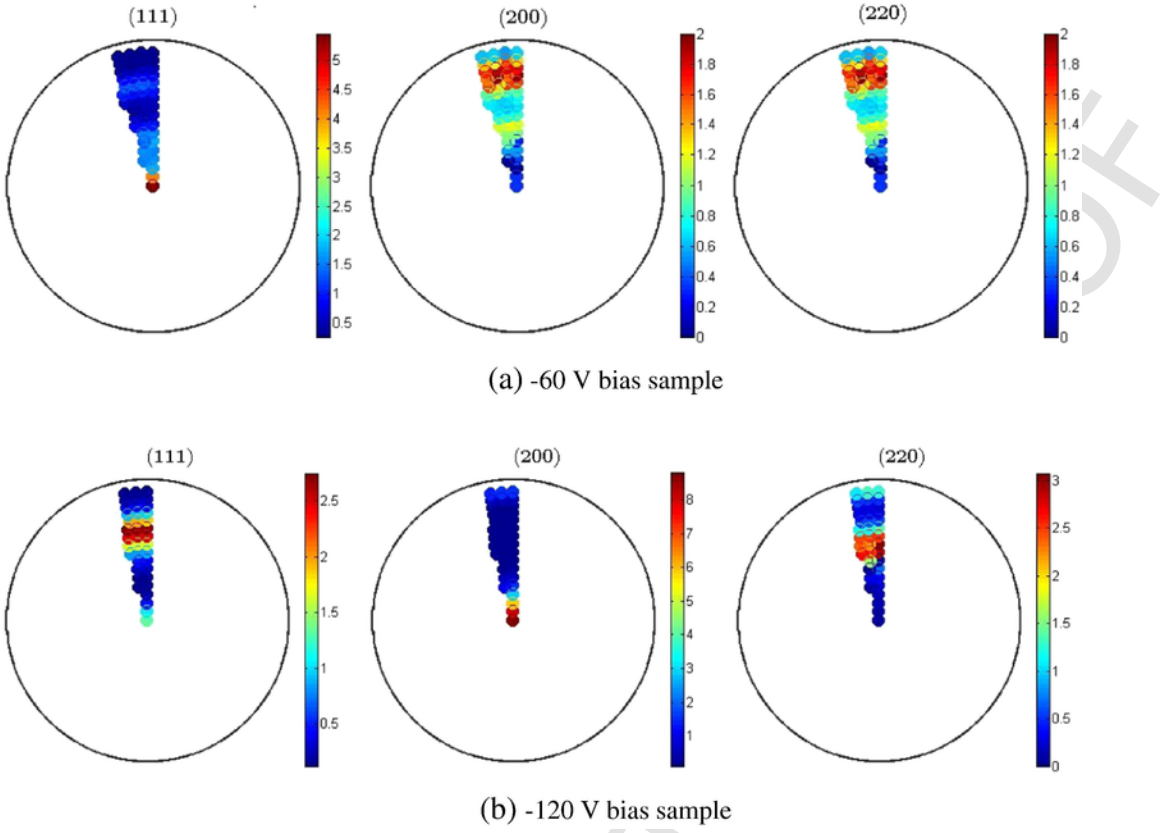

Fig. 8. Pole figures of (a) − 60 V samples (low bias) and (b) − 120 V (high bias) samples; as usual for pole figures, the radial coordinate is the χ angle and the azimuthal coordinate is the φ angle.

high-bias coatings; the latter have a significantly sharper texture than the low-bias ones.

In conclusion, XRD observations clearly show that consistent microstructures can be obtained in the range between − 90 and − 210 V. On this basis, the bias voltage chosen to make the multilayer coatings were − 120 V, − 150 V and − 180 V, to ensure no microstructure disruption during bias switching.

4.2. Nanomechanical characterization (E, H, Kc)

Table 2 highlights the experimental results of the mechanical characterization of the six single-layer coatings made with different biases, while the results for the three multi-layers are reported in Table 3. Elastic modulus and hardness values are presented as the average calculated at an indentation depth of 100 nm; all the results are compatible with previous works like [31].

Table 2
Experimental results of different CrN coatings.

BIAS voltage (− V)	Experimental Modulus (E), GPa	Experimental Hardness (H), GPa	Coating Thickness, μm
60	333.70 ± 27.80	27.65 ± 2.70	3.80 ± 0.20
90	337.90 ± 25.40	25.56 ± 2.87	3.90 ± 0.22
120	336.30 ± 40.40	25.34 ± 4.24	3.90 ± 0.22
150	394.00 ± 65.20	29.95 ± 5.28	4.00 ± 0.25
180	310.40 ± 39.20	23.54 ± 3.29	2.70 ± 0.14
210	316.70 ± 52.40	24.01 ± 4.99	2.70 ± 0.14

A Poisson's ratio (ν) of 0.25 was used for all cases

Table 3
Experimental results of multilayer Cr-CrN coatings.

BIAS voltage (− V)	Experimental Modulus (E), GPa	Experimental Hardness (H), GPa	Coating Thickness, μm
120_120_120	348.10 ± 49.10	25.84 ± 4.81	4.00 ± 0.20
120_150_180	359.70 ± 58.70	26.68 ± 5.26	3.70 ± 0.19
180_150_120	340.60 ± 44.90	24.89 ± 4.34	4.10 ± 0.20

A Poisson's ratio (ν) of 0.25 was used for all cases

The hardness and elastic moduli of all samples are comparable, or at least within the experimental error, pointing to similar stoichiometry and grain size for all coatings. More refined compositional analysis would be required to gain quantitative information on coatings' stoichiometry, which is beyond the scope of this paper.

Fracture toughness values of the samples were obtained using the pillar splitting method [20,21]. Fig. 9a highlights the SEM micrograph of a pillar after fracture, highlighting the effects on interlayers on crack propagation. Fig. 9b shows the fracture toughness values of all the multilayer samples. For comparison, a monolayer sample produced at − 150 V is also shown in the same figure. A small increase of fracture toughness is observed for the three multilayer systems in comparison to monolayers. However, it is clear that the improvement is minor, probably because of the very similar microstructure of the films with respect to the single-layers.

As discussed in previous papers [20,21], The response from pillar splitting experiments is expected to be direction dependent in case of single-crystals and/or strongly textured polycrystalline films. In the present case, all samples showed a similar texture and a grain size

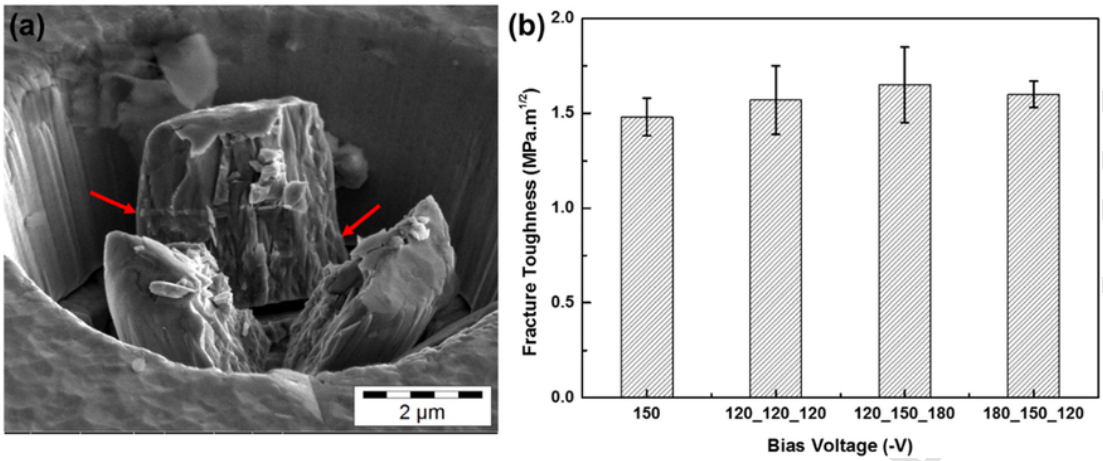

Fig. 9. (a) Representative image of pillar splitting on a multilayer sample, with arrows highlighting the interlayers, (b) Fracture toughness values of different samples, both single layer (150) and multilayers (***120_120_120, 120_150_180, 180_150_120).***

much smaller than the pillars' diameter. Therefore, we can assume that quantitative comparison among different samples can be possible for all the samples investigated in this work.

It is also noteworthy that residual stress has no effect on pillar splitting measurements, since the stress is fully relaxed after pillar milling [20].

In conclusion, mechanical characterization shows that multilayer samples have similar hardness, modulus and slightly higher fracture toughness, compared to single layers.

Therefore, we may assume that differences in terms of scratch and wear behaviour may be attributed to the effects of residual stress more than any other microstructural or mechanical effects.

4.3. Residual stress measurements

Fig. 10 reports the average stresses measured on single layers CrN by both XRD $\sin^2\psi$ and FIB ring core milling techniques. Please note that stress values reported in Fig. 10 have been normalized with respect to film thickness, since we observed lower film thickness for higher bias samples, probably due to a the re-sputtering effect, as reported in previous studies [15,32].

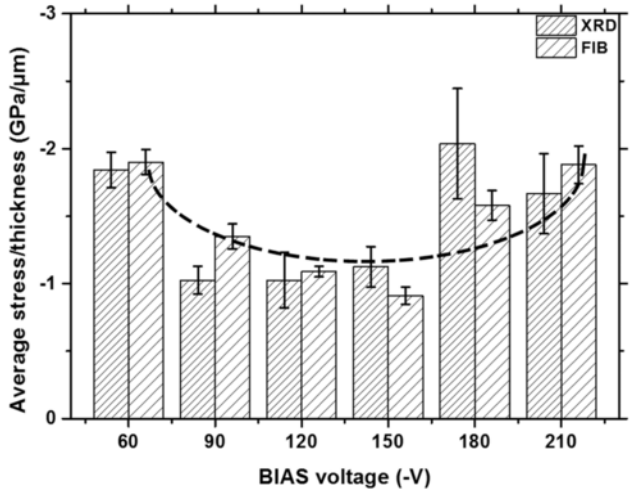

Fig. 10. Normalized residual stresses as a function bias voltage for monolayer samples. The U-shaped line is a guide for the eye to provide better understanding.

Higher average stresses are observed for both low (− 60 V) and high bias (− 210 V). Going from a bias voltage of − 60 V to − 210 V, the stress trend follows a "U" shape trend, with high stress at the lowest and highest biases, and minimum stress in the middle. This behaviour is to be expected at low deposition pressures, due to a large fraction of highly energetic ions from cathode reaching the growing coating. As a results of this, the ion plating system for moderate biases act as a source of heat, capable to anneal the defects induced by the cathode ions [33]. Only at high biases the energy of the locally generated ions become high enough to produce stress and supersede the annealing effect. Conversely, if the deposition is carried out at high enough pressure, the stress plot is often linear, with a rough proportion of stress with bias [33]. There is also a difference between the stress values reported using XRD and the FIB-DIC method. It is well known fact that the XRD measurements strongly depend upon the coating texture, and this effect can be readily assessed in this work checking the difference in error bars between XRD stress for low bias coating and high bias coating. Detailed discussion on the difference of the stress values between XRD and FIB method is reported in a previous paper [34].

Fig. 11 shows the average stress in the three multilayer coatings, as expected the uniform − 120 V bias sample shows the lowest value of residual stress. Two dashed lines on the Fig. 11 represents the average stress values for the monolayer samples produced using a bias voltage of − 120 and − 180 V. Clearly, the average stress values of − 120 V multilayer sample is very similar to the one of monolayer sample produced at the same bias. On the other hand, combining three different biases in the shape of a multilayer brings the value slightly higher than the − 120 V bias, but still significantly lower than the − 180 V bias.

Fig. 12 shows the residual stress profiling in the three multilayer samples, achieved through the incremental ring-core approach [8].

The uniform − 120 V sample (***120_120_120***) show similar stresses at the surface and interface of the coating, showing the highest surface stress and the smallest stress gradient over the thickness.

The sample with higher bias voltage nearby the interface (***120_150_180***) shows the lower value of surface stresses and higher value of interface stresses, as expected.

On the contrary, the sample deposited with lower bias voltage nearby the interface (***180_150_120***), has not the lowest interface stress. A possible explanation for this behaviour is the natural growth tendency of zone-T PVD coatings of having increasing stress towards the interface, since this effect is intrinsically related to the grain

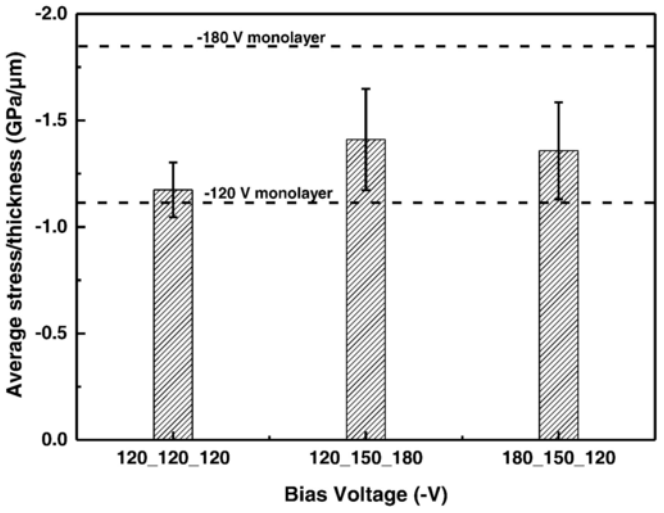

Fig. 11. Average normalized residual stresses in different multilayer coatings, two dotted lines represents the average stress values in the monolayer samples produced using − 120 and − 180 V bias.

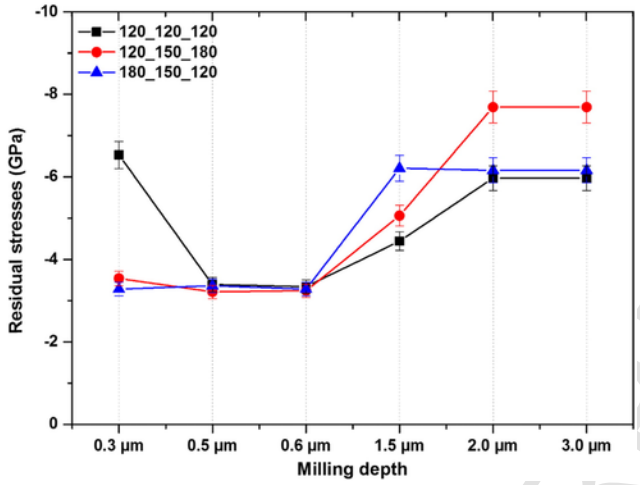

Fig. 12. Residual stress profile in different multilayer coatings using by the incremental ring-core method.

growth process and hence difficult to suppress. At the beginning of the deposition, the grain size and thus the grain boundaries are similar in all cases, so changing the bias has a simple effect on the stress (due to greater or lower flow of adatoms in the grain boundaries). However, increasing the thickness of the coating, the grain growth changes according to the bias history. The coating with constant applied bias (− 120 V in this study) has lowest heating dose by the ion plating system (in an RF ion plating system the power is not proportional to the voltage), and thus, the lowest possibility to anneal the intrinsic stress during growth. This is a possible explanation for the high surface stress for sample (***120_120_120***).

In any case, it is important to note that significant differences among the samples were obtained in terms of stress profiles, which can be correlated to scratch resistance as reported in the following section.

4.4. Scratch testing

Scratch testing results using a 200 μm indenter on single-layer coatings are summarized in Fig. 13.

Comparing the complete delamination values with the normalized stresses reported in Fig. 10, it is quite clear that presence of higher average stresses reduces the delamination load and hence affecting the adhesion of the coating with the substrate. This is probably because of buckling in the films for higher average compressive stresses. Therefore, it is confirmed that compressive residual stress can be beneficial in coatings up to a certain limit, when buckling in the films can be induced during sliding contact. This is also confirmed by the analytical simulation results reported in Fig. 3, where lower average stress of the film with a slightly increasing stress towards the interface are predicted for a 200 μm indenter radius.

Fig. 14 shows the adhesion testing on the multilayer coatings using a 200 μm indenter. First of all, it is clear that adhesion of all multi-layer coatings is significantly higher than any of the produced

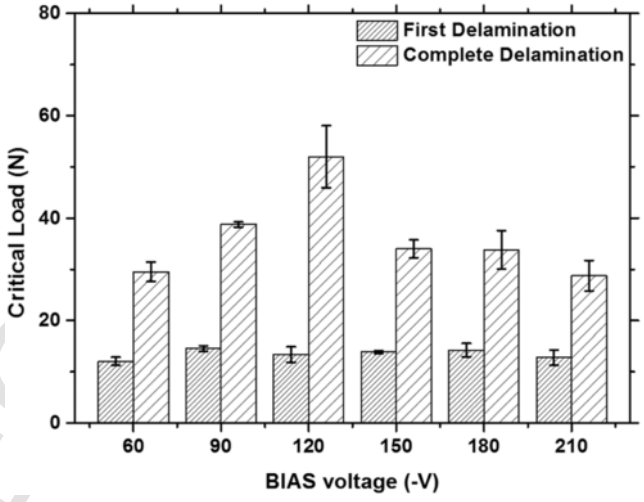

Fig. 13. Scratch test results on single layer coatings using 200 μm indenter.

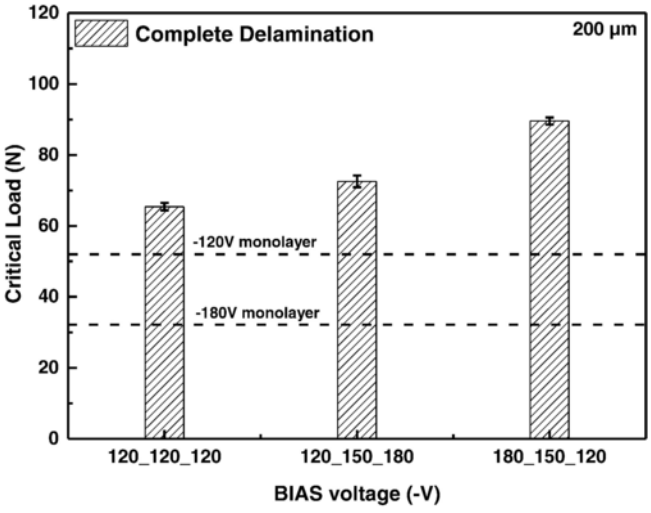

Fig. 14. Scratch test results on multilayer coatings using 200 μm indenter, the dotted lines highlight the values for the monolayer coatings using the same indenter.

single layers. This is probably because of the beneficial effect of the ductile metal layers in optimising the contact stress distribution, promoting re-nucleation of the CrN layers and controlling crack propagation paths, as reported in previous papers [35–37].

At the same time, a significant difference is also observed among the three multi-layers, which only differ for the residual stress state. In fact, the sample with lowest interface stress and the lowest stress gradient (***180_150_120***) shows significantly higher critical load for adhesive failure, with respect to sample with highest interface stress (***120_150_180***), according to FIB-DIC stress measurements.

This experimental results are in good agreement with the FilmDoctor simulations; the software predicted better performance for coatings with low stress gradient and 4–5 GPa of average stress, like in the samples presented here. Testing the same coatings with a 10 μm indenter gives different results between the samples (Fig. 15). Although the ***180_150_120*** still shows higher values of adhesion, the multilayer coating with the higher compressive stresses at the surface (***120_120_120)*** demonstrated improved adhesion when tested with the sharper 10 μm indenter.

This is a confirmation that optimal stress profiles in films should be always referred to a specific loading condition, where lower contact radii require higher surface stress.

These results are also in accordance with the FilmDoctor simulations, Fig. 2, which show that smaller the indenter radius higher the stresses required at the surface of the coatings and the interface; given that the natural gradient for T zone coating is high in the interface and low in the surface, using a high bias on the surface can allow to maintain the stress high through all the thickness, giving high enough compressive force to all layers. A major role has to be ascribed to the plastic deformation of the ductile substrate (AISI 304 stainless steel): during the scratch test the contact stress in the coating is much lower thanks to the plastic deformation (in FilmDoctor the substrate is a perfectly elastic material, so the simulation can be assumed as reliable only until the von Mises stress in the substrate cross the yielding threshold). The difference in performance between the monolayer and the multilayer cannot be explained only by higher toughness of the multilayer samples, given the results of pillar indentations that show an intrinsic toughness of the multilayer samples only somewhat higher than the monolayer samples. The difference between the monolayer and multilayer should be ascribed to the stress profile modification given by the metallic interlayers.

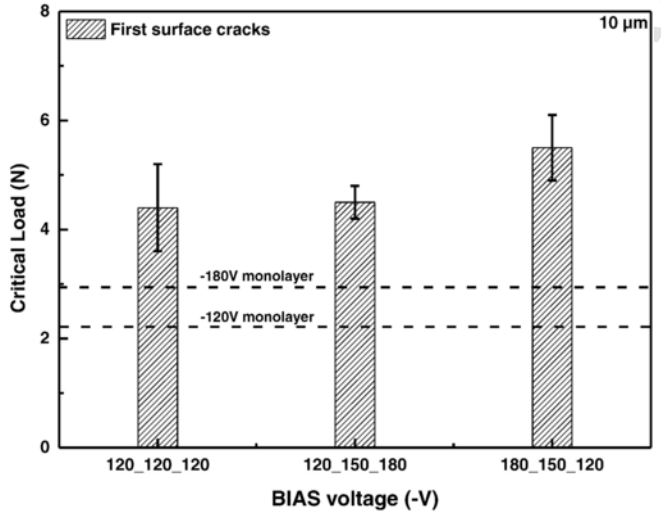

Fig. 15. Scratch test results on multilayer coatings using 10 μm indenter, the dotted lines show the values for the monolayer coatings using the same indenter.

5. Conclusion

The aim of this work was to put forward evidence for the possibility to design a coating with improved adhesion by tailoring the residual stress profiles, without changing significantly its hardness and modulus. The results of the simulations point out clearly that changing tip radius and applied load involves a modification of the optimal (desired) residual stress profile in the film.

Using results from modelling, multilayer coatings with different stress profiles, but similar hardness and microstructure, were produced and characterised.

Stress profiles were measured by incremental micro-scale FIB-DIC method, showing significant differences among the three multilayer samples, and demonstrating a clear correlation between the observed stress gradient and scratch adhesion behaviour.

In particular, coatings with reduced interfacial residual stress show significantly higher adhesion, as obtained by using both a 200 μm and 10 μm radius of the diamond indenter; at the same time, coatings with higher surface stress show an improved performance when using a sharper 10 μm indenter.

Such results demonstrate that the optimal gradients of residual stress may change, depending on the radius of the counterpart and should be carefully considered for the design of multilayer coatings with improved adhesion.

Acknowledgments

Authors would like to thank Daniele de Felicis for technical assistance during FIB experimentation at the interdepartmental laboratory of electron microscopy (LIME) of University of "Roma TRE", Rome, Italy. The financial support for this work (M Renzelli, M Z Mughal and M Sebastiani) was provided through the European FP7 Project, iSTRESS (Grant # 604646, www.istress.eu).

References

[1] H.O. RW, S. Preissler, Residual stresses in nitride hard coatings prepared by magnetron sputtering and arc evaporation, Surf. Coat. Technol. 74-75 (1995) 273–278.
[2] H.K.T.B.K.A.M.H. Seegers, Influence of stress distribution on adhesion strength of sputtered hard coatings, Thin Solid Films 332 (1998) 146–150.
[3] H. Oettel, R. Wiedemann, Residual stresses in PVD hard coatings, Surf. Coat. Technol. 76-77 (1995) 265–273.
[4] H.K.T.H. Seegers, Influence of residual stress gradients on the adhesion strength of sputtered hard coatings, Thin Solid Films 377-378 (2000) 340–345.
[5] X.L. Peng, T.W. Clyne, Mechanical stability of DLC films on metallic substrates: part I—film structure and residual stress levels, Thin Solid Films 312 (1998) 207–218.
[6] V. Teixeira, Mechanical integrity in PVD coatings due to the presence of residual stresses, Thin Solid Films 392 (2001) 276–281.
[7] V. Teixeira, Residual stress and cracking in thin PVD coatings, Vacuum 64 (2002) 393–399.
[8] M. Sebastiani, C. Eberl, E. Bemporad, G.M. Pharr, Depth-resolved residual stress analysis of thin coatings by a new FIB–DIC method, Mater. Sci. Eng. A 528 (2011) 7901–7908.
[9] A.M. Korsunsky, M. Sebastiani, E. Bemporad, Focused ion beam ring drilling for residual stress evaluation, Mater. Lett. 63 (2009) 1961–1963.
[10] A.M. Korsunsky, M. Sebastiani, E. Bemporad, Residual stress evaluation at the micrometer scale: analysis of thin coatings by FIB milling and digital image correlation, Surf. Coat. Technol. 205 (2010) 2393–2403.
[11] E. Salvati, T. Sui, A.J.G. Lunt, A.M. Korsunsky, The effect of eigenstrain induced by ion beam damage on the apparent strain relief in FIB-DIC residual stress evaluation, Mater. Des. 92 (2016) 649–658.
[12] R. Ali, M. Sebastiani, E. Bemporad, Influence of Ti–TiN multilayer PVD-coatings design on residual stresses and adhesion, Mater. Des. 75 (2015) 47–56.

[13] N. Schwartzer, The extended Hertzian theory and its uses in analysing indentation experiments, Philos. Mag. 86 (2006) 5179–5197.
[14] http://siomec.de.
[15] C. Rebholz, H. Ziegele, A. Leyland, A. Matthews, Structure, mechanical and tribological properties of nitrogen-containing chromium coatings prepared by reactive magnetron sputtering, Surf. Coat. Technol. 115 (1999) 222–229.
[16] NPL. Determination_of_Residual_Stresses_by_X-ray_Diffraction_-_Issue_2 NPL Guides.
[17] F. Bachmann, R. Hielscher, H. Schaeben, Texture analysis with MTEX – free and open source software toolbox, Solid State Phenom. 160 (2010) 63–68.
[18] R. Hielscher, H. Schaeben, A novel pole figure inversion method: specification of theMTEXalgorithm, J. Appl. Crystallogr. 41 (2008) 1024–1037.
[19] W.C. Oliver, G.M. Pharr, Improved technique for determining hardness and elastic modulus using load and displacement sensing indentation experiments, J. Mater. Res. 7 (1992) 1564–1580.
[20] M. Sebastiani, K.E. Johanns, E.G. Herbert, F. Carassiti, G.M. Pharr, A novel pillar indentation splitting test for measuring fracture toughness of thin ceramic coatings, Philos. Mag. 95 (2015) 1928–1944.
[21] M. Sebastiani, K.E. Johanns, E.G. Herbert, G.M. Pharr, Measurement of fracture toughness by nanoindentation methods: recent advances and future challenges, Curr. Opinion Solid State Mater. Sci. 19 (2015) 324–333.
[22] M.Z. Mughal, R. Moscatelli, M. Sebastiani, Load displacement and high speed nanoindentation data set at different state of charge (SoC) for spinel LixMn2O4 cathodes, Data in Brief 8 (2016) 203–206.
[23] M.Z. Mughal, R. Moscatelli, H.-Y. Amanieu, M. Sebastiani, Effect of lithiation on micro-scale fracture toughness of LixMn2O4 cathode, Scr. Mater. 116 (2016) 62–66.
[24] C. Eberl, R. Thompson, D. Gianola, W. Sharpe Jr, K. Hemker, Digital Image Correlation and Tracking. MatLabCentral, Mathworks File Exchange Server, FileID, 12413, 2006.
[25] G. Schajer, Measurement of non-uniform residual stresses using the hole-drilling method. Part I—stress calculation procedures, J. Eng. Mater. Technol. 110 (1988) 338–343.
[26] G. Schajer, Measurement of non-uniform residual stresses using the hole-drilling method. Part II—practical application of the integral method, J. Eng. Mater. Technol. 110 (1988) 344–349.
[27] J.A. Thornton, High rate thick film growth, Annu. Rev. Mater. Sci. 7 (1977) 239–260.
[28] R. Daniel, K.J. Martinschitz, J. Keckes, C. Mitterer, The origin of stresses in magnetron-sputtered thin films with zone T structures, Acta Mater. 58 (2010) 2621–2633.
[29] Q. Kong, L. Ji, H. Li, X. Liu, Y. Wang, J. Chen, et al., Influence of substrate bias voltage on the microstructure and residual stress of CrN films deposited by medium frequency magnetron sputtering, Mater. Sci. Eng. B 176 (2011) 850–854.
[30] L. Cunha, M. Andritschky, K. Pischow, Z. Wang, Microstructure of CrN coatings produced by PVD techniques, Thin Solid Films 355–356 (1999) 465–471.
[31] H.N. Shah, R. Jayaganthan, A.C. Pandey, Nanoindentation study of magnetron-sputtered CrN and CrSiN coatings, Mater. Des. 32 (2011) 2628–2634.
[32] G. Bertrand, C. Savall, C. Meunier, Properties of reactively RF magnetron-sputtered chromium nitride coatings, Surf. Coat. Technol. 96 (1997) 323–329.
[33] K.J. Martinschitz, R. Daniel, C. Mitterer, J. Keckes, Stress evolution in CrN/Cr coating systems during thermal straining, Thin Solid Films 516 (2008) 1972–1976.
[34] E. Bemporad, M. Brisotto, L.E. Depero, M. Gelfi, A.M. Korsunsky, A.J.G. Lunt, et al., A critical comparison between XRD and FIB residual stress measurement techniques in thin films, Thin Solid Films 572 (2014) 224–231.
[35] R. Daniel, M. Meindlhumer, J. Zalesak, B. Sartory, A. Zeilinger, C. Mitterer, et al., Fracture toughness enhancement of brittle nanostructured materials by spatial heterogeneity: a micromechanical proof for CrN/Cr and TiN/SiOx multilayers, Mater. Des. 104 (2016) 227–234.
[36] M. Bartosik, M. Arndt, R. Rachbauer, C. Krywka, C.M. Koller, J. Keckes, et al., Cross-sectional X-ray nano-diffraction and -reflectivity analysis of multilayered AlTiN–TiSiN thin films: correlation between residual strain and bi-layer period, Scr. Mater. 107 (2015) 153–156.
[37] M. Stefenelli, R. Daniel, W. Ecker, D. Kiener, J. Todt, A. Zeilinger, et al., X-ray nanodiffraction reveals stress distribution across an indented multilayered CrN–Cr thin film, Acta Mater. 85 (2015) 24–31.